Effect of Areal Density and Fiber Orientation on the Deformation of Thermomechanical Bonds in a Nonwoven Fabric

Joseph Rittenhouse,[1] Roshelle Wijeratne,[2] E. Bruce Orler,[3] David A. Dillard,[4] Robert B. Moore,[3] Raffaella De Vita[5]

[1]*Department of Materials Science and Engineering, Virginia Tech, Virginia 24060*
[2]*Department of Mechanical Engineering, Virginia Tech, Virginia 24060*
[3]*Department of Chemistry, Virginia Tech, Virginia 24060*
[4]*Department of Biomedical Engineering and Mechanics, Virginia Tech, Virginia 24060*
[5]*STRETCH Lab, Department of Biomedical Engineering and Mechanics, Virginia Tech, Virginia 24060*

This study proposes a novel method to mechanically characterize the performance of individual bonds in low-density, thermomechanically bonded nonwoven fabrics. Commercial bicomponent, polyethylene/polypropylene (PE/PP), nonwoven fabric was laser cut into bowtie-shaped specimens for uniaxial tensile testing so that the central region of each specimen contained an individual bond. Three groups, each composed of 20 specimens, were tested with their longitudinal axes oriented along the machine direction (MD), the cross direction (CD), and at 45° between these two directions (DD). Prior to testing, the intrinsic variation in areal density and fiber orientation in the region surrounding the individual bond were quantified via orientation and relative basis weight parameters. During testing, images of the specimens were acquired to determine the occurrence of fiber breakage, bond deformation, and bond cohesive failure. Maximum force, stiffness, and orientation parameters were found to be significantly different among the three specimen groups ($p < 0.01$) but the relative basis weight was not ($p > 0.01$). The stiffness and maximum load were linearly correlated with both the areal density and fiber orientation. Pre-existing voids or windows within the bond lowered the maximum force for specimens with the longitudinal axes aligned with the MD. These voids had no influence on the maximum force achieved by the specimens aligned with the CD and DD. The bonds in these specimens were observed to deform less than the bonds in the specimens with the longitudinal axes aligned with the MD. The results indicate the importance of the fiber structure surrounding the bond on the tensile properties, deformation and failure mode of individual bonds within the nonwoven fabric. POLYM. ENG. SCI., 59:311–322, 2019. © 2018 Society of Plastics Engineers

INTRODUCTION

The global market for spunbond nonwoven fabrics is growing rapidly and expected to reach over $50 billion by 2020 [1]. This growth can be attributed to nonwoven's numerous applications, ease of manufacturing, and customizable properties such as fabric stiffness, extensibility, and composition. Such fabrics find a wide range of use spanning from automotive and construction fields to medical, consumer, and technology industries. Spunbond nonwoven fabric is produced by depositing extruded, spun fibers onto a moving collecting belt. The speed of the belt in relation to the extrusion speed imparts directionality to the fibers and determines the density of the fabric [2]. The fibers are then joined by mechanical, chemical, or thermal means to form localized bonds [3]. The most common bonding process is the thermomechanical bonding process that involves subjecting the fibrous mat to pressure and heat under an embossed calender roll. The bonds are the key structural elements of nonwovens imparting the stiffness, strength, and the integrity that are needed for subsequent manufacturing processes that depend on the final applications of the nonwovens.

Industrial producers can create nonwovens with a range of mechanical properties by controlling processing parameters such as bonding temperature, bonding pressure, and fiber characteristics. Unfortunately, producers have limited ability of predicting the performance of the nonwovens under various loading scenarios that are encountered in different applications. The current Edisonian approach of a trial and error manufacturing process requires significant amounts of raw material and many hours of production time. Therefore, studying how thermomechanical bonds and the fibers surrounding such bonds influence the final performance of the entire nonwoven fabric is of significant importance to the nonwovens industry.

The formation of thermomechanical bonds in nonwovens occurs in three stages [4]. First, a web of fibers is compressed and heated. During this stage, the fiber surfaces come into full contact with each other while the temperature is increased. Usually, the temperature is close to the melting temperature of the polymer used to ensure sufficient flow. Second, the web is point-bonded. The fibers reach an elevated temperature underneath (oftentimes) discrete calender nips. The increase in temperature causes melting of the crystalline structure of the fibers. This provides mobility that permits surface conformation and polymer molecular interdiffusion across the fiber interface, thereby allowing contacting fibers to join. The polymer molecular interdiffusion is dependent on the temperature, pressure from nips, and time duration at the elevated pressures and temperatures [5–7]. Third, the bonded web of fibers cools. During this stage, the bonds solidify with recrystallization, thus becoming mechanically stable. The fibers in the web may be multicomponent, consisting of two or more polymer constituents that behave uniquely due to different melting temperatures, viscosities, and crystalline structures.

Correspondence to: R. De Vita; e-mail: devita@vt.edu
DOI 10.1002/pen.24907
Published online in Wiley Online Library (wileyonlinelibrary.com).

Several investigators have characterized the mechanical properties of the entire nonwoven fabrics by testing specimens containing multiple bonds. More specifically, the effects of polymer morphology and polymer type on the mechanical properties of the nonwoven fabrics have been investigated [4, 8, 9]. Most of the published research has been on polyolefins, specifically polypropylene [2, 4, 10] Notably, Kim et al. [11] determined the failure modes for nonwoven specimens (15 cm $\times$ 2.5 cm) made from isotactic polypropylene fibers at various bonding temperatures and pressures. By performing uniaxial tests, they found that the dominant mode of failure was fiber/fiber interfacial failure within the bonds at lower bonding temperatures and bond–fiber junction failure at higher bonding temperatures.

Damage of nonwoven fabrics is dependent on the fiber-to-bond junctions. There are multiple studies on the mechanical properties of the constituent fibers of the nonwoven prior to bonding [2, 8, 12–15]. Faruhk et al. [16] examined how morphological differences affected the mechanical properties of polypropylene fibers entering a bond. These investigators created a procedure for measuring the loss in the tenacity of fibers by tensile testing single fibers between two clamped bonds. Their findings revealed that the strength of bonded fibers in the nonwoven was 50% less than that of the virgin unbonded fibers. According to the researchers, this was likely the result of polymer morphology gradients at the fiber-to-bond junction. This gradient was experimentally characterized by Wang et al. [17], who concluded that the polymer morphology of the bond was considerably different from that of the virgin fiber through Raman microspectroscopy.

The local structure and uniformity of nonwovens significantly influence the global nonwoven mechanical properties. Hou et al. [18] showed that intrinsic variation within nonwoven fabrics, such as areal fiber density, affected the nonwoven deformation. Tensile tests and image analysis indicated that stress concentrated in local regions with low fiber density and transferred from one low fiber density region to another one, generating shear stresses within the specimen. These areas of nonuniform fiber density can vary within only a length of 2.0 mm. Rawal et al. [19–22] conducted considerable theoretical and experimental work to determine the effect of fiber orientation, fiber volume fraction, number of fiber-to-fiber contacts, distance between the contacts, and porosity on the mechanical behavior of thermally bonded nonwoven fabrics. The results indicated the influence of the local fiber structure on the global mechanical properties of the nonwovens. They found good agreement between their theoretical model, incorporating global measurements of areal density and fiber directions, and experimental results. Furthermore, Amiot et al. [23] provided correlations of fiber structure parameters to tensile, air permeability, and compression measurements. All above-cited studies have suggested the importance of considering the mechanical properties of localized regions within the nonwoven fabrics.

Many mechanical models have been proposed to describe the material behavior of the thermomechanically bonded nonwovens. In the models for nonwovens, the bonds are treated as rigid bodies or as composites whose properties are calculated from bicomponent virgin fiber properties [24–29]. The rigid body assumption on the bonds leads to inaccurate predictions due to the significant strain experienced by the bonds [30]. Additionally, properties of a single bond calculated from virgin fiber properties do not account for local variations in structure or morphological variations due to bonding parameters, such as bonding temperature and pressure. Subsequently, models based on rigid body and composite assumptions may not provide the most accurate predictions of both the global and local mechanics of the nonwovens. The bonds, which are typically less than 1.0 mm $\times$ 1.0 mm and inhomogeneous, deform, and exhibit local failure mechanisms that are different from those observed globally in the bulk material [19, 31, 32]. Consequently, there is a need to characterize the mechanical performance of individual bonds and, at the very least, the local mechanical behavior of the nonwovens.

The focus of this study is to develop novel experimental methods to determine the mechanical behavior, including the failure mode, of single bonds within a nonwoven fabric by accounting for the local fiber structure surrounding the bond. Toward this end, specimens containing single bonds are isolated from a commercially produced nonwoven. The specimens are analyzed for fiber density and fiber orientation in the regions surrounding the bonds and are then tested uniaxially. The results will help practitioners understand, and eventually predict, the integrity of the bonds within nonwovens, including the role of the local fiber structure. The outcome of this study could have significant implications in the manufacturing process of nonwovens and lead to more efficient use of the industrial resources such as time and raw materials, while producing more viable products.

MATERIALS AND METHODS

Specimen Preparation

Commercially produced bicomponent spunbond nonwoven fabric, made of polyethylene/polypropylene (PE/PP) fibers deposited at a nominal areal density of 20 g m^{-2}, was obtained from a commercial roll-goods supplier. Four sheets of spunbond fabric, $\sim$20 cm $\times$ 28 cm, were used: one was used only for relative basis weight analysis and three for relative basis weight analysis, fiber orientation analysis, and tensile testing.

Three of the four sheets were laser cut into 120 bowtie specimens using a laser cutter (Epilog Mini 24 laser, Golden, CO) set at rasta/vector, 90% speed, and 10% power. There was no attempt to register these fabrics with respect to the cutting pattern. An example of one bowtie specimens, 4.5 mm $\times$ 22.5 mm, is shown in Fig. 1a. Specimens with bonds centered within their gage regions were deemed suitable for testing while the rest of the specimens were discarded. The central position of the bond ensured load transfer through the bond during tensile testing. More precisely, the laser was only used to cut the clamping regions of the specimens and medical shears were used to isolate the bond in order to prevent damage of the bond due to heat from the laser or additional welding of surrounding fibers. This provided a consistent geometry for the specimens, with notches that helped localize bond failure while allowing free movement of the surrounding fibers.

The bowtie specimens were cut with their longitudinal axes along three different directions in regards to the entire nonwoven fabric: machine direction (MD), cross direction (CD), and at

 DOI 10.1002/pen

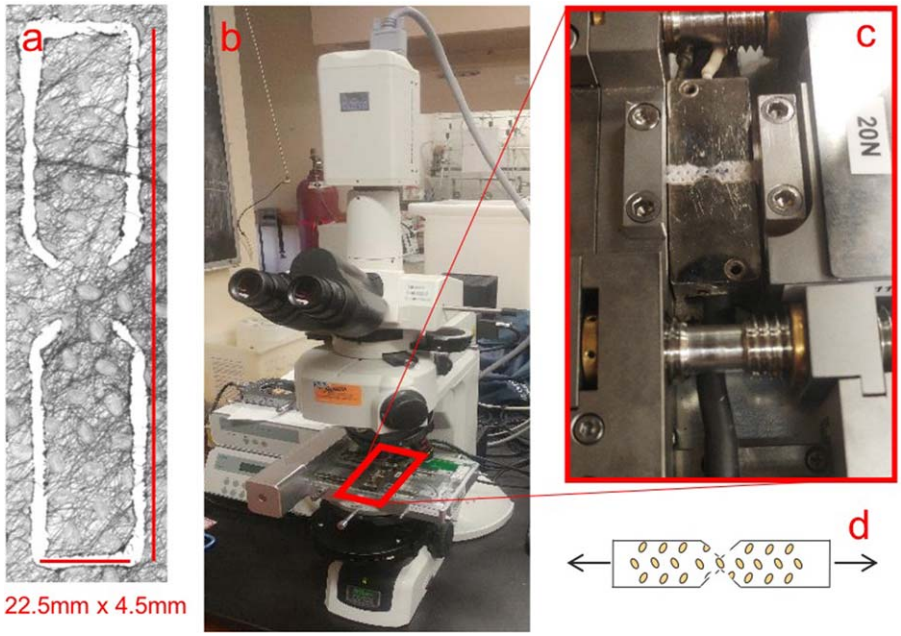

FIG. 1. (a) Digital scan of a bowtie specimen for tensile testing with the bond in the central region. (b) Microscope, camera and tensile stage used for testing. (c) Tensile stage with clamped specimen. (d) Schematic of bowtie specimen and loading direction. [Color figure can be viewed at wileyonlinelibrary.com]

45° between these two directions. This latter direction will be called the diagonal direction (DD). Each sheet of fabric was used to isolate a total of 20 acceptable bowtie specimens ($n = 20$) with their longitudinal axes along the same direction (MD, CD, or DD).

Relative Basis Weight and Fiber Orientation

Four spunbond nonwoven sheets were scanned using an optical transmission scanner (Epson Perfection V850 Pro) at a scanning resolution of at least 2,400 dpi. A total of 10,000 squares ~1.5 mm × 1.5 mm were randomly selected from the non-laser-cut nonwoven sheet to measure the relative basis weight. Both relative basis weight and fiber orientation were measured for the specimens isolated for tensile testing from three of the laser cut nonwoven sheets using ImageJ software (National Institute of Health; Bethesda, MD). More specifically, square areas ~1.5 mm × 1.5 mm inside the notched regions of the bowtie specimens that contained bonds in their centers were selected for these measurements.

Relative basis weight was calculated using the Beer–Lambert law [31], according to which the intensity of light transmitted through the nonwoven is given by

$$I = I_0 e^{-\mu\rho L}, \tag{1}$$

where I_0 is the intensity of incident light, μ is the mass-absorption coefficient, L is the thickness of the nonwoven, and ρ is the density of the nonwoven. As ρL is the mass per unit area, or basis weight (B), *Eq. 1* is modified as

$$I = I_0 e^{-\mu B} \tag{2}$$

and *Eq. 2* can also be written as

$$B = \frac{1}{\mu} ln\left(\frac{I_0}{I}\right). \tag{3}$$

Equation 3 can be used to determine basis weight of the nonwoven at any location based on a given I_0, I, and μ [33]. I_0 and I were measured from the transmission scanner in regions without and with the nonwoven material present, respectively. However, the mass absorption coefficient μ was not readily measurable or available. Therefore, only the relative basis weight, B_{relative}, of different regions within the same nonwoven were compared by computing the values of $B\mu$:

$$B_{\text{relative}} = B\mu = ln\left(\frac{I_0}{I}\right). \tag{4}$$

If no material was present, then the resulting relative basis weight was zero (i.e. the ratio of I_0 and I is unity). As the amount of material increased, so did the relative basis weight. Consequently, it was possible to compare relative basis weights of different regions (e.g., regions A and B) within the same nonwoven sheet in regards to the amount of light transmitted. If a region A and a region B had relative basis weights of 0.50 and 0.25, respectively, then there was twice as much mass in region A compared to region B.

The fiber orientation distribution surrounding the bond of each specimen that was mechanically tested was computed by determining the direction of the intensity gradient [34]. The analysis was done using the OrientationJ plugin (École Polytechnique Federale De Lausanna; Lausanna, Switzerland). The scanned image was first aligned along the specimen's tensile axis corresponding to 0° in the software and then filtered to smooth the image to remove any fine scale details, especially any undesirable fine scale topography on the bond surface within the width of a fiber diameter. This was accomplished by

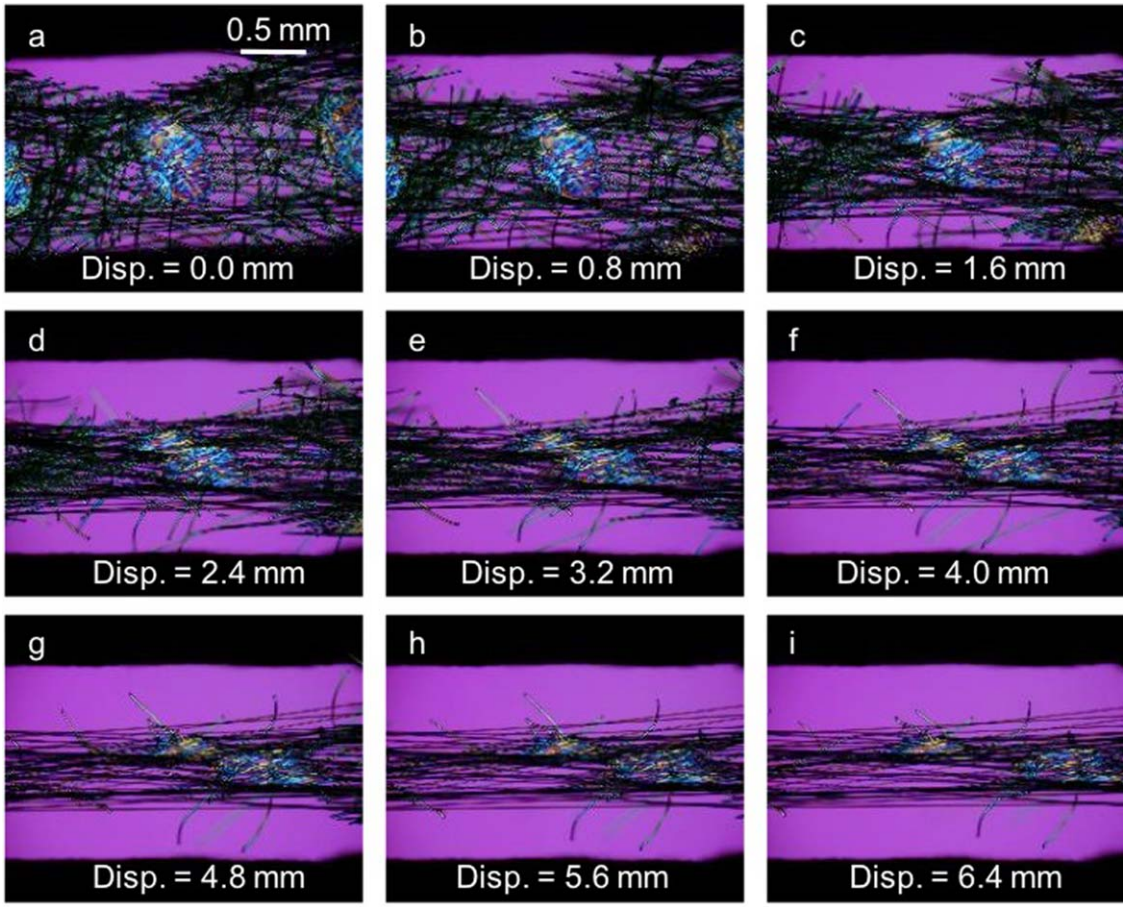

FIG. 2. Micrographs of a representative bowtie specimen with its loading axis aligned along the MD at different displacement values (from 0.0 to 6.4 mm) illustrating bond deformation and a cohesive shearing failure. [Color figure can be viewed at wileyonlinelibrary.com]

running a Gaussian Blur procedure at the fiber diameter of 17 μm.

Given the orientation distribution, an orientation parameter, O_p, was calculated. The orientation angle, θ, of each fiber was measured with respect to the longitudinal direction of the bowtie specimens. After defining the orientation distribution as $f(\theta)$, the following *Equation* from Cox's analysis strength of fibrous materials [35] was used to determine the orientation parameter:

$$O_p = \frac{\int_{-\pi/2}^{\pi/2} f(\theta) cos^4(\theta) d\theta}{\int_{-\pi/2}^{\pi/2} f(\theta) d\theta}. \quad (5)$$

It is important to note that 0° was defined as the longitudinal direction of the specimens that coincided with the axial loading direction. This choice led to orientation parameter values between zero and unity, where zero indicated that the fibers were aligned perpendicular to the loading direction and unity indicated that the fibers were aligned along the loading direction.

Uniaxial Tensile Testing

Specimens ($n = 60$) were loaded into a tensile stage (Linkam TST350, 20 N load cell with 0.01 N resolution) attached to a microscope (Nikon Eclipse LV100) (Fig. 1b and c). During mechanical testing, the microscope was set to 40× magnification view with automatic image capturing at every 2 s. The specimen was illuminated from below with cross-polarization and a quarter-wave shift. This light scheme was chosen to image both fibers and bond throughout testing. The specimens were preloaded to 0.01 N prior to data acquisition. This ensured that all specimens started from similar loading conditions. Each specimen was tested at a constant extension rate of 40 μm s^{-1} at room temperature.

Force and displacement data were collected together with corresponding images of the specimen. For each specimen, the stiffness and maximum force were calculated. The stiffness was determined by considering the force–displacement data collected from the specimens stretched up to 0.3 mm displacement. This region of the force–displacement curve was determined to be representative of the initial linear elastic region for all specimens. The mean and standard deviation (SD) of stiffness over $n = 20$ specimens were also computed for each testing direction (MD, CD, and DD).

The image sets were analyzed to observe individual bonds and three modes of failure were visually detected. Prior to starting the tensile test, the specimens were classified as having whole bonds or partial bonds, that is, bonds with voids or windows created during the production process. Once the test started, the images were analyzed for fiber breakage, bond

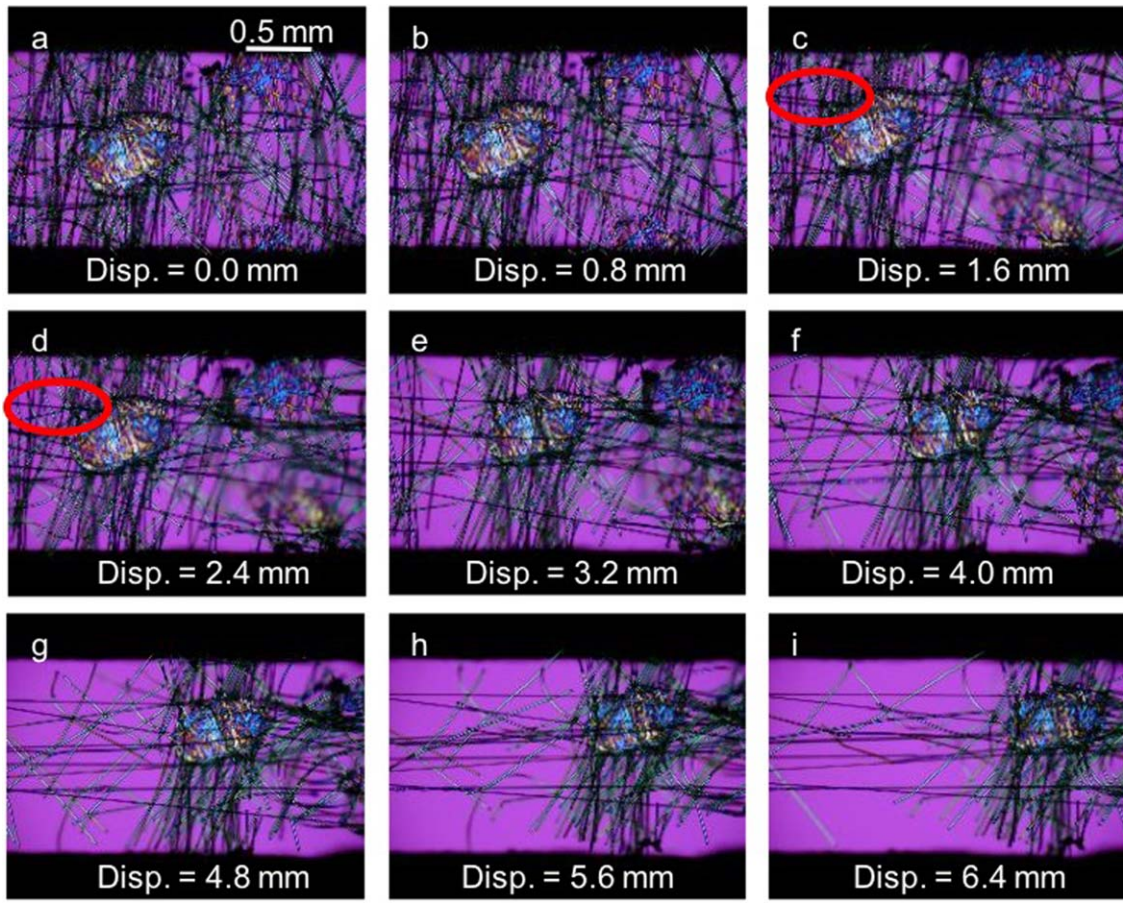

FIG. 3. Micrographs of a representative bowtie specimen loaded along the CD at different displacement values (from 0.0 to 6.4 mm) illustrating fiber breakage and no bond deformation. The red circles in (c) denote the presence of two fibers and in (d) the breakage of one of these two fibers. [Color figure can be viewed at wileyonlinelibrary.com]

deformation, and bond cohesive failure. A visually detected change in bond geometry was interpreted as bond deformation. Fiber breakage indicated the breakage of an individual fiber. Last, bond cohesive failure denoted failure of the bond itself (e.g., tearing of a bond into two or more parts).

Statistical Analysis

The means and standard deviations were calculated for the maximum load, stiffness, orientation parameter, and basis weight ($n = 20$) for specimens in the MD, CD, and DD. They were compared statistically using ANOVA. Additionally, means and standard deviations were calculated for maximum load and stiffness for specimens having bonds with and without voids the MD, CD, and DD. The Student's t test was used to compare the differences between these quantities. The threshold for statistical significance was chosen to be 0.05. Statistical analysis was performed in Excel.

RESULTS AND DISCUSSION

The bowtie specimens loaded along the MD often experienced failure within the bond under tensile loading, likely because there were more fibers in the axial direction capable of transmitting load to the bond. Figure 2 shows a representative image set for these specimens. More precisely, Fig. 2a presents the central region of the specimen at the start of the tensile test (gage displacement was 0.0 mm) after the specimen was preloaded to 0.01 N. Multiple colors can be observed within the bond due to the cross polarization. This difference in colors indicates heterogeneity of molecular orientation within the polymer chains. If the bond were perfectly homogeneous, with all of polymer chains in the bond oriented in only one direction, then the bond would be one single color. This high degree of heterogeneity was present in all of the bonds studied. In each of following images (Fig. 2b–i) the original gage length of 15 mm increased by 0.8 mm over a time interval of 20 s. As the load increased, the bond reoriented itself along the loading direction and deformed significantly in this direction (Fig. 2c). In Fig. 2d, one can observe that the bond sheared along a line roughly parallel to the loading direction and separated in two parts. This indicated the occurrence of cohesion failure of the bond. After such failure (Fig. 2i), the bowtie specimen was successfully supporting load despite the bond having fractured into two separate parts since there were still many fibers supporting the load. Cohesive failure that propagated along the fiber direction, such as in Fig. 2, may be due to the polyethylene fused fiber sheath having failed while the polypropylene fiber core maintained structural integrity. This type of bond deformation and failure was commonly observed for specimens with their longitudinal axis aligned along the MD. Most importantly, the bond allowed

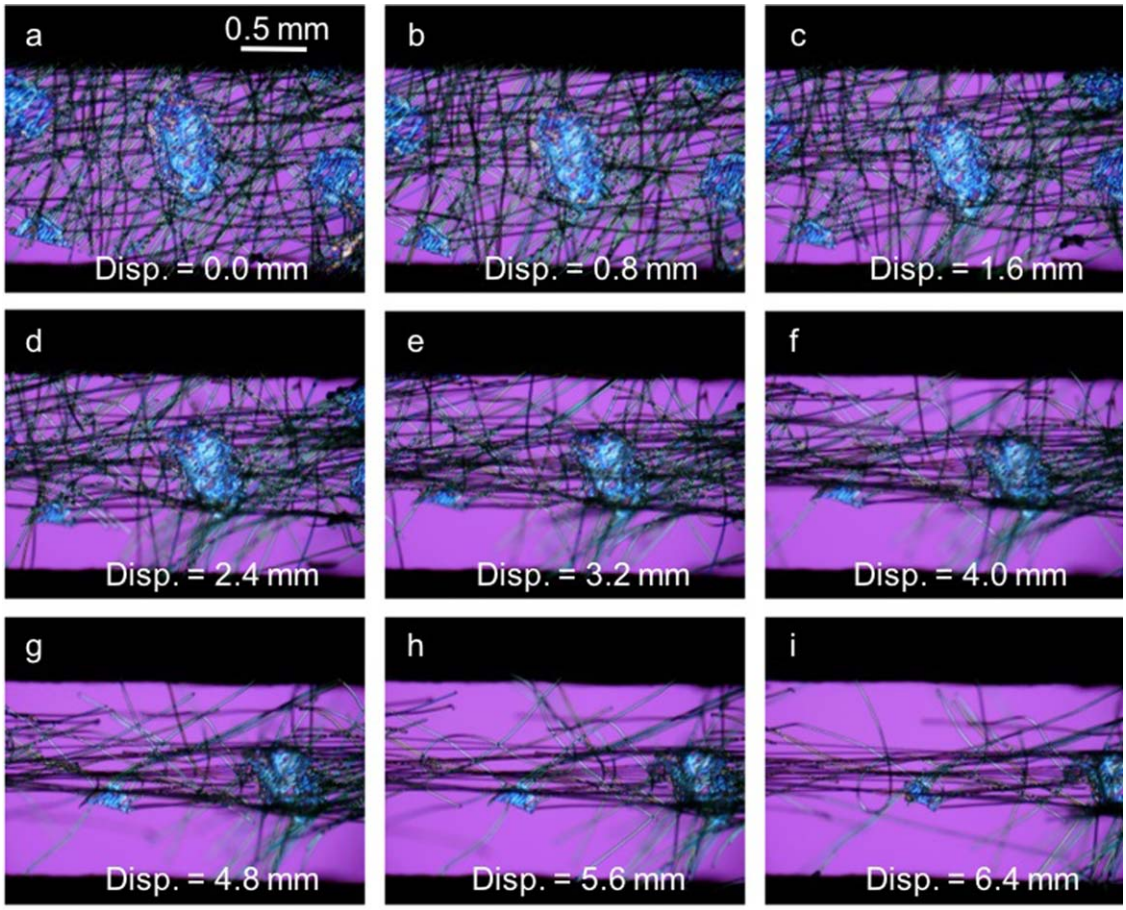

FIG. 4. Micrographs of a representative bowtie specimen loaded along the DD at different displacement values (from 0.0 to 6.4 mm) illustrating fiber breakage and minimal bond deformation. [Color figure can be viewed at wileyonlinelibrary.com]

distribution of load to multiple fibers. Usually, at a 6.4 mm displacement (Fig. 2i), fiber failure was not detected for specimens in the MD group. This was very different from what was observed for bowtie specimens loaded along the CD, as discussed next.

The specimens subjected to uniaxial tensile tests along the CD displayed individual fiber failure with no visible bond deformation. Figure 3 presents an image set for a representative specimen that was loaded along the CD. The images were collected from the start of the test, at 0.0 mm displacement, up to a 6.4 mm displacement. Although the load increased, the bond did not deform or reorient significantly (Fig. 3c), in contrast to what occurred for the specimen loaded in the MD (Fig. 2c). In Fig. 3c, fibers transferring load within the bond can be observed. Then, in Fig. 3d, fewer fibers transferring load can be detected. This indicates individual fiber failure. After a displacement of 2.4 mm, the number of fibers attached to one site of the bond decreased and the fibers on such site deformed more. The bond no longer had a comparable number of fibers attached to its opposite sites along the CD. When the displacement was 6.4 mm (Fig. 3i), there were fewer than 10 fibers applying load on one side of the bond, and the bond did not display any noticeable deformation. It was uncommon for the bond to deform visibly or to experience cohesive failure for the specimens loaded along the CD. Individual fiber breakage was the primary mode of failure for these specimens, even at gage displacements as low as 2.4 mm (Fig. 3d). These specimens had noticeably fewer fibers oriented along the loading axis that entered the bond than the specimens tested in the MD, likely reducing the load that was applied to the bonds.

The specimens that were tensile tested along the DD primarily experienced individual fiber breakage with minimal bond reorientation and deformation. Figure 4 shows an image set for a representative specimen loaded along the DD. Again, images were collected as described above. The bond did not appear to deform or reorient significantly at 1.6 mm displacement (Fig. 4c), similarly to the bonds within the specimens loaded along the CD. As the displacement increased (Fig. 4f), the visual size of the bond decreased as the bond curvature changed. Visually, there was no significant in-plane bond deformation or cohesive failure. Similar to what occurred for the specimens loaded along the CD (Fig. 3), the bond did not have an equal number of fibers on its opposite sites. Additionally, the number of fibers attached to the bond decreased as the displacement increased indicating fiber breakage (Fig. 4f–i).

The wide range of bond characteristics resulted in specimens that exhibited significantly different mechanical behaviors. Figure 5 displays a specimen tested along the MD that was extremely different than the previously shown representative specimen (Fig. 2). One can observe that, due to the low density

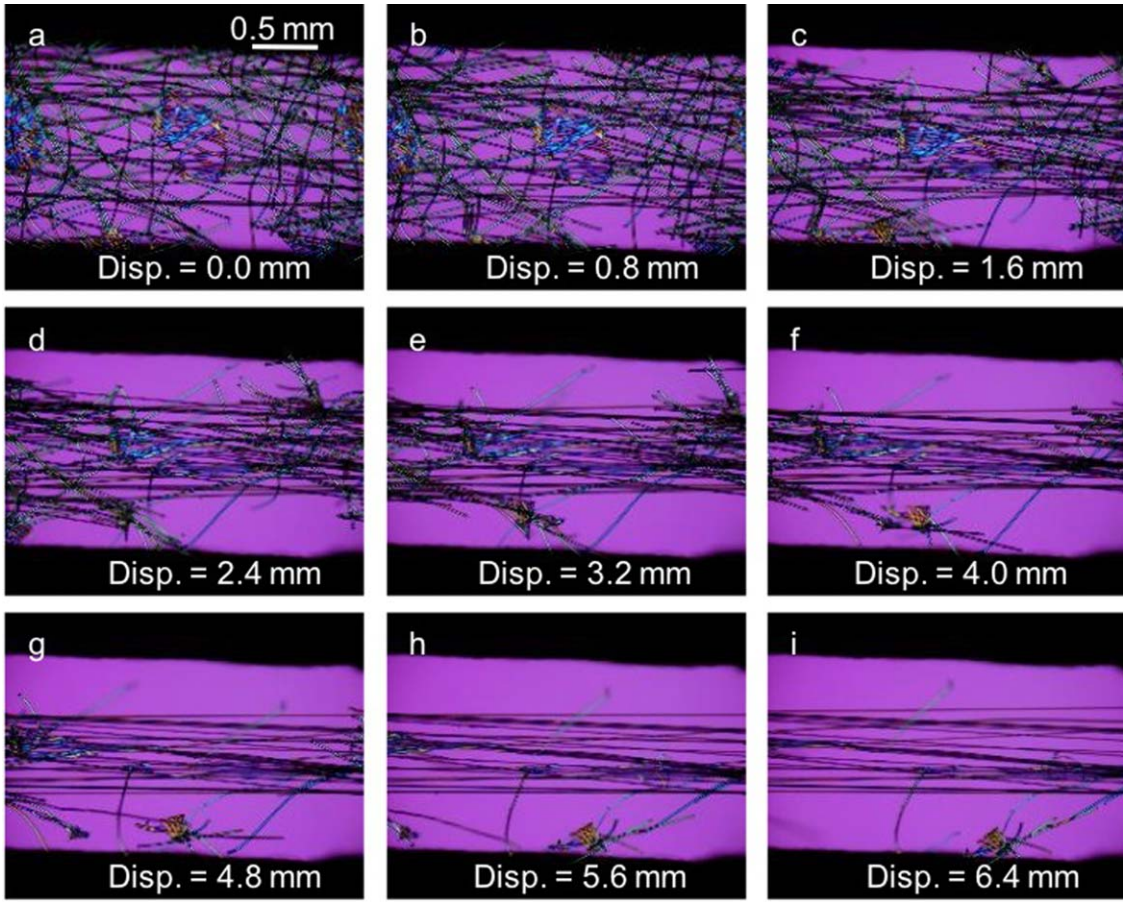

FIG. 5. Micrographs of a bowtie specimen loaded along the MD at different displacement values (from 0.0 to 6.4 mm) illustrating how the variability in the specimen structure (e.g., lack of fibers within the bond or presence of voids within the bond) led to bond deformation and failure mechanisms that were different from those usually observed for specimens in the MD group (Fig. 4). [Color figure can be viewed at wileyonlinelibrary.com]

of fibers, the bond was partial and not fully formed. Many voids or windows were present. Significant bond deformation was visible at 2.4 mm displacement (Fig. 5d) and the bond nearly disintegrated at 5.6 mm displacement (Fig. 5h). This was different from what happened for the representative specimen tested along the MD, which exhibited significant bond deformation after a displacement of 6.5 mm (Fig. 2). This high degree of variation was evident when the quantitative mechanical data collected from each specimen were compared.

The ability of a bond to support load was greatly affected by the bond and fiber orientation relative to the axial loading direction. However, as shown in Figs. 2 and 5, even within specimens loaded along the same direction, there was a large degree of variation in mechanical response. Figure 6a displays the mean and standard deviations of the load versus displacement data for bowtie specimens with their longitudinal axes oriented along the three directions, MD, CD, and DD. The maximum load for the specimens tested along the CD was slightly >0.1 N, but attained 0.2 N for the specimens tested along the DD and extended beyond 0.4 N for the specimens tested along the MD. Similarly, the stiffness was the highest for specimens in the MD group and lowest for specimens in the CD group as can be seen by the slope of the initial linear region of the load–displacement curves (Fig. 6b) ($p < 0.05$). The role of the fiber orientation on the mechanical properties has been previously studied for the entire nonwoven fabrics by other investigators [23, 30, 36, 37]. These studies detailed failure of specimens with multiple bonds, whereas this study confirmed the importance of fiber orientation on the load of an individual bond. Furthermore, the results revealed a significant variation for specimens with their longitudinal axes aligned along the same direction, such as the MD. This variation suggests the need for local fiber orientation measurements *versus* global orientation measurements of the whole fabric. The intrinsic variation of force–displacement data within low-density nonwoven fabric studied can be, in part, understood when considering the different failure mechanisms of the tested specimens.

While the force–displacement data were found to depend on the loading direction, individual bonds displayed unique failure mechanisms that depended on their original structure. In Table 1, the total number of specimens, the number of specimen with partial bonds (bonds with voids or windows), and the number of specimens that experienced (i) fiber failure, (ii) bond deformation, and (iii) bond cohesive failure are reported. As indicated in Table 1, fiber failure was observed in all the specimens at some point during the test. Typically, specimens in the MD group displayed fiber failure after 6.4 mm displacement while specimens in the CD and DD groups displayed such failure mode before

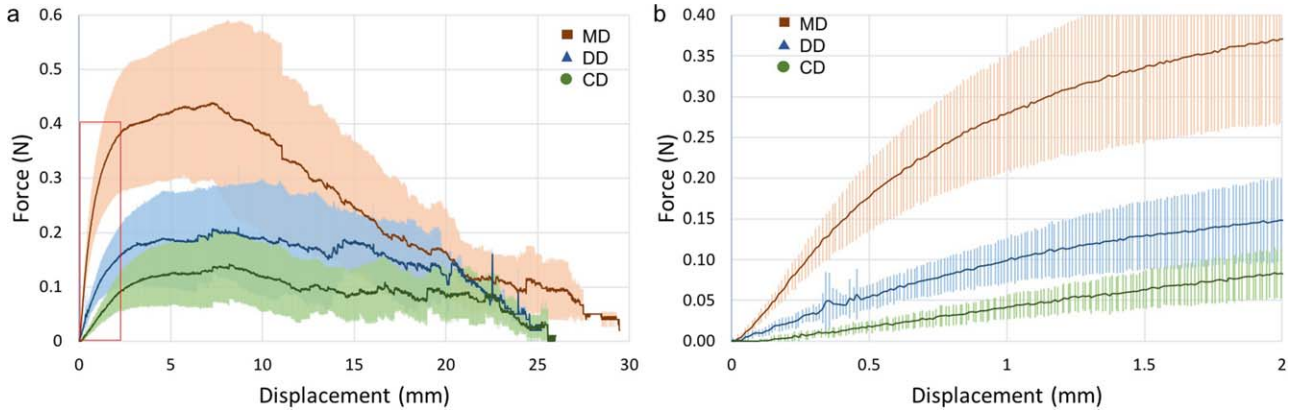

FIG. 6. (a) Average force *versus* displacement curves with standard deviations collected from specimens tested along the MC ($n = 20$), DD ($n = 20$), and CD ($n = 20$). (b) Average force versus displacement curves up to 0.4 N force and 2 mm displacement as indicated by the red box in (a). [Color figure can be viewed at wileyonlinelibrary.com]

reaching 6.4 mm displacement. On the other hand, failure modes varied among specimens and the following correlations were noted:

- Half of the specimens with their longitudinal axes oriented along the MD contained bonds with visible voids or windows, yet nearly all the bonds appeared to deform. This was likely due to the numerous fibers that were aligned along the axial loading direction and thus transferred load into the bond. Because of these fibers, the specimens were able to sustain forces that were high enough to deform the bonds.
- The presence of pre-existing voids or windows lowered the average maximum force that was achieved for specimens loaded along the MD by ~35%. Specimens without voids reached an average force of 0.581 ± 0.085 N while specimens with voids only reached an average force of 0.379 ± 0.118 N. These maximum forces were found to be statistically different ($p < 0.05$). The voids could have served as stress concentrators, or the reduced number of fibers may simply have resulted in a lower force sustained by the specimens.
- The presence of pre-existing voids also influenced whether bonds within specimens loaded along the DD and CD deformed visibly. Due to reduced material and/or stress concentrations associated with voids within a bond, fewer fibers were required to transfer the forces needed to deform the individual bond. Consequently, pre-existing voids typically correlated with visible bond deformation.
- Interestingly, the impact of voids on the maximum force achieved by the specimens was less influential for specimens loaded along the DD and CD. For the DD group, the force changed by ~30%, going from 0.273 ± 0.109 N for specimens without voids to 0.182 ± 0.074 N for specimens with voids. However, this difference was still statistically significant ($p < 0.05$). For the CD group, there was no appreciable difference in the maximum force which was 0.153 ± 0.068 N for specimens without voids and 0.148 ± 0.060 N for specimens with voids ($p > 0.05$). Again, with fewer fibers oriented along the loading axis for these specimens, bond failure likely occurred due to the failure of the fibers that made up the bond.
- Bonds within all specimens with pre-existing voids displayed higher likelihood of cohesive failure. In fact, none of the fully formed bonds (i.e., bonds without voids or windows) that were tested displayed cohesive failure.

These qualitative observations indicated the importance of the density and orientation of fibers in and around individual bonds on the mechanical response of the bond. Moreover, the nonuniformity within the tested low-density spunbond fabric was so high that it was necessary to accurately quantify the local variation.

The fiber orientation of spunbond nonwoven fabrics has been used widely to understand the mechanical behavior of these fabrics. However, fiber orientation has typically been calculated as a global property by scanning large areas of fabrics without accounting for the local fiber orientation, that is the fiber orientation within the region of the specimens selected for mechanical testing [9, 38]. In this study, variations in fiber orientation that occurred over relatively small length scales were found to be significant (Fig. 7). Figure 7a illustrates how the fiber orientation changed depending on the size of the area analyzed. For the same specimen, the fiber orientation of a large area (a global measurement) containing the bond in question, such as 10.0 mm × 6.0 mm area, was significantly different from the fiber orientation of a small area (a local measurement) containing only the bond and the surrounding area. Figure 7b displays the fiber orientation distributions for individual bonds in the MD ($n = 20$). The distributions were all centered near 0°; however, the spread of the distribution changed significantly among specimens. The maximum frequency and shape of each distribution was unique to the individual specimen. This variation was also found for the specimens with their longitudinal axes along the DD, as shown in Fig. 7c, and for the specimens with their longitudinal axes along the CD, in Fig. 7d.

TABLE 1. Number of bowtie specimens with the longitudinal axes aligned along the MD, CD, and DD are reported. For each group, number of specimens with bonds having voids or windows as well as the observed occurrence of fiber failure, bond deformation, and bond cohesive fracture are reported.

Direction	Number of specimens	Number of specimens with partial bonds	Number of specimens experiencing		
			Fiber breakage	Bond deformation	Bond cohesive failure
MD	20	10	20	19	7
DD	20	9	20	8	6
CD	20	8	20	7	4

DOI 10.1002/pen

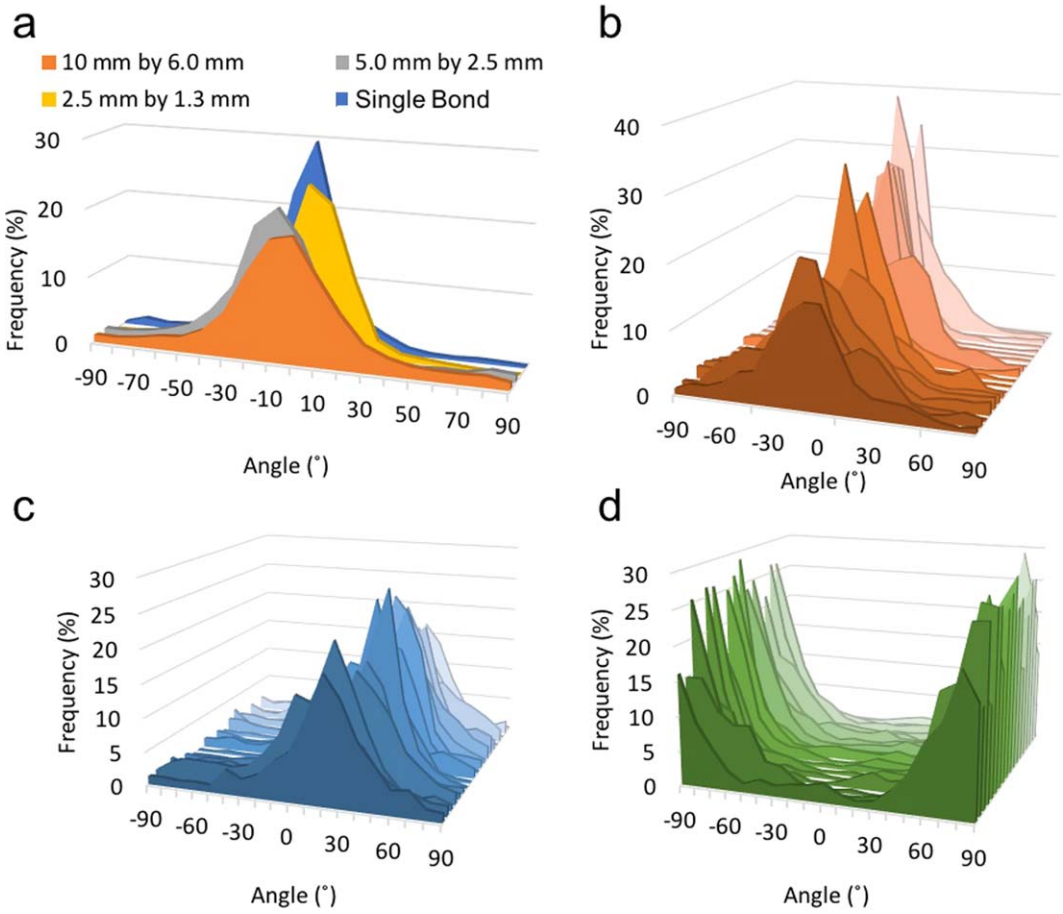

FIG. 7. (a) Change in fiber orientation distribution depending on the size of the area selected for scanning. Four areas of different sizes are selected from the same region within a single specimen ($n = 1$). (b), (c), (d) Fiber orientation histograms for specimens with their longitudinal axis in the MD ($n = 20$), DD ($n = 20$), and CD ($n = 20$), respectively. [Color figure can be viewed at wileyonlinelibrary.com]

There was extreme variation in the relative basis weight, which ranged from 0.16 to 0.76. Relative basis weight was used to measure the relative density of fibers surrounding a bond. Figure 8 shows the two frequency histograms binned at every 0.01 from 0.00 to 1.00. The continuous (grey) region represents 10,000 relative basis weight measurements from a full fabric

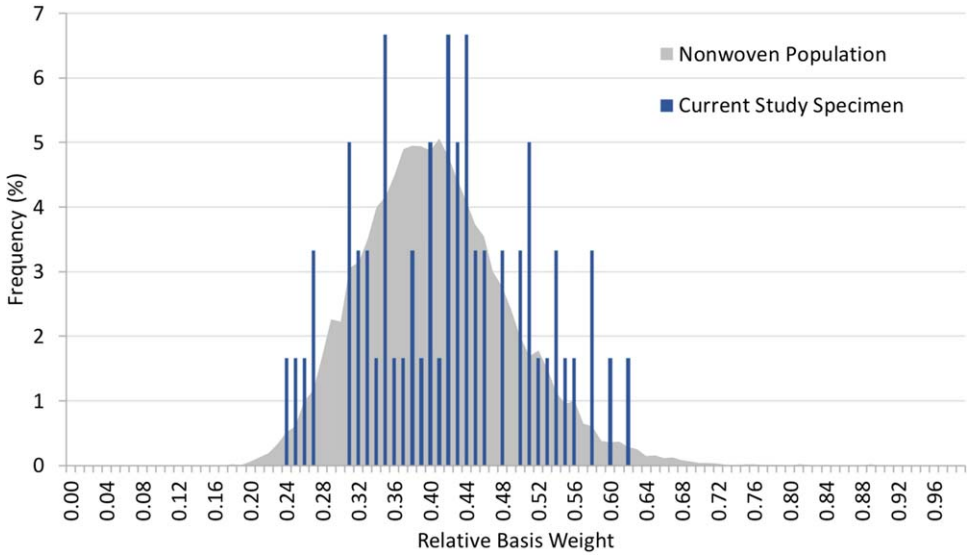

FIG. 8. Distribution frequency of relative basis weights calculated from one nonwoven sheet and from the specimens ($n = 60$) that were mechanically tested. [Color figure can be viewed at wileyonlinelibrary.com]

TABLE 2. Averages and standard deviations of measured quantities computed over $n = 20$ bowtie specimens with their longitudinal axes oriented along the MD, DD, and CD.

Direction	Stiffness (N/mm) (0.1–0.3 mm)	Maximum load (N)	Orientation parameter	Relative basis weight
MD	0.360 ± 0.086	0.489 ± 0.138	0.772 ± 0.102	0.405 ± 0.097
DD	0.109 ± 0.035	0.232 ± 0.103	0.190 ± 0.048	0.416 ± 0.096
CD	0.043 ± 0.017	0.155 ± 0.063	0.078 ± 0.029	0.461 ± 0.083

sheet and the discrete (blue) histogram shows relative basis weight measurements from all specimens used in this study. The 10,000 relative basis weight measurements confirmed that the specimens chosen were representative of the entire nonwoven fabric sheet.

Table 2 presents the averages and standard deviations for stiffness, maximum load, orientation parameter, and relative basis weight for specimens with their longitudinal axes oriented along the MD, CD, and DD. As already mentioned, the stiffness and maximum load were significantly different across the three groups of specimens ($p < 0.05$). The average orientation parameter was also significantly different across the three groups of specimens ($p < 0.05$). It was the highest for specimens with their longitudinal axes in the MD, lower for those with their longitudinal axes along DD, and lowest for those with their longitudinal axes in the CD. This was expected since, when making the nonwoven fabrics, the deposited fibers have some preferred orientation along the MD because of the speed of the moving web. The average relative basis weights were similar for the three groups of specimens. Statistical analysis proved that the relative basis weights in the MD, CD, and DD were not significantly different ($p > 0.05$). Nevertheless, it is important to note that one standard deviation from the mean can change the relative basis weight from ~0.3 to 0.5.

The local fiber orientation in combination with the number of fibers surrounding a bond influenced the resulting mechanical behavior of the specimens. Figure 9a shows a linear correlation between the stiffness and the product of the orientation parameter and relative basis weight. The stiffness of the specimens was low when there were few fibers and the fibers were not aligned along the axial loading direction. When the total number of fibers increased and more fibers were aligned with the axial loading direction, the specimens' stiffness increased. For the specimens with their longitudinal axis aligned along the MD, the stiffness increased from 0.25 to 0.50 N mm^{-1} and linearly correlated to the alignment of fibers with the loading direction and the density of fibers surrounding the bond. Similarly, the maximum load increased as the fibers aligned with the loading direction and the total number of fibers increased as shown in Fig. 9b. Consequently, the ability to transfer the load through the bond was attributed to the number of fibers (relative basis weight) and the alignment of those fibers to the loading direction (fiber orientation parameter). These data demonstrated how the initial fibrous structure surrounding the bond determined the load that the bond could sustain even after significant displacement (>5.0 mm) of the specimen.

The data reported in Fig. 9a and b indicated that the intrinsic variation in the stiffness and maximum load of the bonds in nonwoven fabrics can be reduced by considering the local fiber orientation and relative basis weight. Thus, discerning the influence of various manufacturing processing parameters on the mechanical performance of a bond would be extremely difficult without accounting for variations in the local fiber orientation and density.

In this study, force and displacement data were collected to evaluate the mechanical behavior of the bonds. Although stress and strain data are needed to compute the mechanical properties of the bonds, the discontinuous nature of the specimens prevented their measurements. Indeed, the width of the specimens varied along the length of each specimen due to voids or windows in the bonds and empty space among fibers. Similarly, strain could not be computed for the entire duration of the tests due to individual fiber failure and bond failure. In our previous study [39], we attempted to compute strain of individual bonds in a nonwoven under biaxial testing by manually tracking the displacement of ink particles placed on the bonds and using the digital image correlation (DIC) method. However, the discontinuous nature of the bonds and their failure during biaxial testing

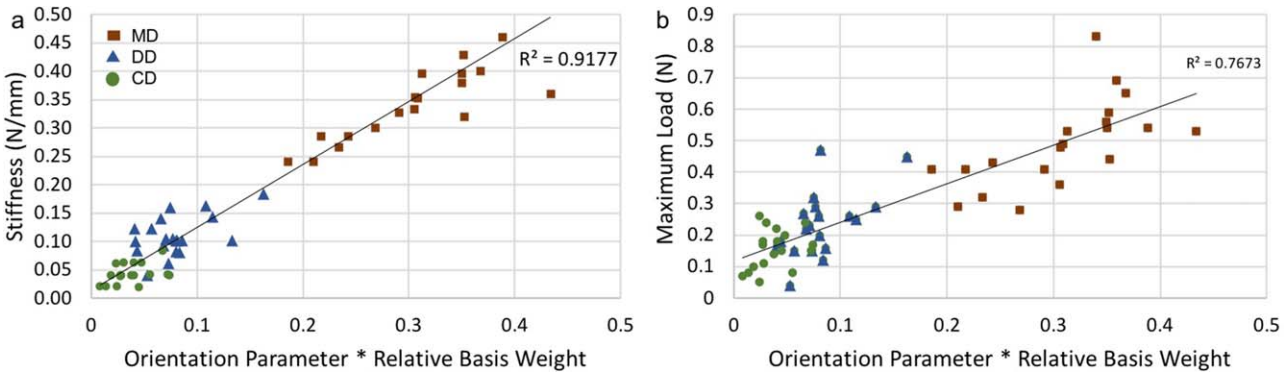

FIG. 9. (a) Orientation parameter multiplied by relative basis weight parameter *versus* stiffness. (b) Orientation parameter multiplied by relative basis weight parameter *versus* maximum load. [Color figure can be viewed at wileyonlinelibrary.com]

 DOI 10.1002/pen

limited the applicability of the DIC methods to small continuous regions of the bonds and to the initial portion of the biaxial tests before fibers and bonds started to fail.

CONCLUSIONS

This research proposes a novel method for analyzing the mechanical properties of individual bonds in low-density, thermomechanically bonded nonwovens. By laser cutting commercial nonwoven fabrics into specimens of bowtie shaped geometry, individual bonds were examined optically by a through-light scanner and then mechanically tested by performing uniaxial tensile tests. The bowtie specimens were isolated with their longitudinal axes along three different directions in regards to the nonwoven: machine direction (MD), cross direction (CD), and at 45° between these two directions, diagonal direction (DD). By using image capture during tensile testing, different modes of failure of the bonds were also determined and correlated with the fiber organization around the bonds.

Through-light scanning provided a quick local measurement of fiber areal density (relative basis weight) and fiber orientation, indicating a high degree of variation in the fiber organization surrounding individual bonds. Most notably, even for specimens with the longitudinal axes oriented along the same direction, such as the MD, the local fiber structure surrounding the bond varied significantly. The relative basis weight within the specimens in the MD group varied from 0.25 to 0.63 while the calculated orientation parameter varied from 0.57 to 0.89. Similarly, the local fiber orientation distribution surrounding a bond differed from the global fiber orientation distribution. This suggests that results from global measurements, which include multiple bonds, are not sufficient to determine the mechanical behavior of individual bonds accurately.

Both qualitative and quantitative measurements indicated the importance of the local fiber structure of the bond to its mechanical behavior. Nearly all the specimens in the MD group displayed deformation of the bond during tensile testing, despite the variation of local fiber structure. This was likely due to the high number of fibers in the loading direction that allowed the load to be transfer and deform the bond. Conversely, only bonds with voids deformed for the specimens with their longitudinal axes along the CD and DD. Partial bonds, that is, bonds with voids or windows, in all the specimens of the three (MD, DD, and CD) groups displayed a higher likelihood of cohesive failure than fully formed bonds. Specimens having bonds with lower basis weight and fewer fibers aligned along the loading direction had a lower stiffness and maximum load. As the basis weight and fiber orientation increased, even in a single specimen group (MD, DD, or CD), the stiffness and maximum load increased. Consequently, the variation in the structural properties of specimens from low density thermomechanically bonded nonwoven fabrics can be reduced by accounting for basis weight and fiber orientation.

This research demonstrates how the intrinsic variation of bonds within low-density nonwovens may lead to thermomechanical bonds having different mechanical responses. Understanding the influence of the local fiber structure on the mechanical behavior of individual bonds can assist in determining the performance of the entire nonwoven fabrics as they undergo subsequent manufacturing processes. Thermomechanical bonds are key structural elements imparting the final integrity of the nonwoven fabrics and their performance in various applications. Thus, more efforts should be devoted to study the effect of processing parameters (e.g., temperature) on the bonds in nonwoven fabrics. The next step of this research will be to systematically examine how these processing parameters alter the mechanical behavior of the thermomechanical bonds.

ACKNOWLEDGMENTS

The authors would like to acknowledge the Institute for Critical Technology and Applied Science (ICTAS) and the Macromolecules Innovation Institute at Virginia Tech for their assistance and use of facilities. This work could not have been completed without the generous support from the departments of Biomedical Engineering and Mechanics, Chemistry, and Materials Science and Engineering at Virginia Tech.

REFERENCES

1. *The Future of Global Nonwovens Markets to 2020*. Smithers Pira Market Intelligence (2015).
2. B. Zhao, *Polym. Eng. Sci.* (2017). doi:10.1002/pen.24690s
3. S. Backer, and D.R. Petterson, *Textile Res. J*., **30**, 704 (1960).
4. S. Michielsen, B. Pourdeyhimi, and P. Desai, *J. Appl. Polym. Sci*., **99**, 2489 (2006).
5. R.P. Wool, B.-L. Yuan, and O.J. McGarel, *Polym. Eng. Sci*., **29**, 1340 (1989).
6. Y.H. Kim and R.P. Wool, *Macromolecules*, **16**, 1115 (1983).
7. R.P. Wool, *Polymer Interfaces: Structure and Strength*, Hanser (1995).
8. M. Dasdemir, B. Maze, N. Anantharamaiah, and B. Pourdeyhimi, *J. Mater. Sci*., **47**, 5955 (2012).
9. R.K. Dharmadhikary, H. Davis, T.F. Gilmore, and S.K. Batra, *Textile Res. J*., **69**, 725 (1999).
10. R. Jubera, A. Ridruejo, C. González, and J. LLorca, *Mech. Mater*., **74**, 14 (2014).
11. H.S. Kim, B. Pourdeyhimi, P. Desai, and A.S. Abhiraman, *Textile Res. J*., **71**, 965 (2001).
12. B. Zhao, *Polym. Eng. Sci.* (2017). doi:10.1002/pen.24687
13. S. Mukhopadhyay, *Adv. Filament Yarn Spin. Text. Polym*., 113 (2014).
14. A.R. Osta, C.R. Picu, A. King, O. Isele, R. Hamm, and A. Dreher, *Polym. Int*., **63**, 1816 (2014).
15. F. Farukh, E. Demirci, M. Acar, B. Pourdeyhimi, and V.V. Silberschmidt, *J. Phys. Conf. Ser*., **382**, 012018 (2012).
16. F. Farukh, E. Demirci, M. Acar, B. Pourdeyhimi, and V.V. Silberschmidt, *J. Mater. Sci*., **48**, 2334 (2013).
17. X. Wang and S. Michielsen, *Text. Res. J*., **71**, 475 (2001).
18. X. Hou, M. Acar, and V.V. Silberschmidt, *J. Mater. Sci*., **46**, 307 (2011).
19. A. Rawal and S.K. Agrahari, *J. Mater. Sci*., **46**, 4487 (2011).
20. A. Rawal, A. Priyadarshi, N. Kumar, S.V. Lomov, and I. Verpoest, *J. Mater. Sci*., **45**, 6643 (2010).
21. A. Rawal, A. Priyadarshi, S.V. Lomov, I. Verpoest, and J. Vankerrebrouck, *J. Mater. Sci*., **45**, 2274 (2010).
22. A. Rawal, P.K. Mishra, and H. Saraswat, *J. Mater. Sci*., **47**, 2365 (2012).

23. M. Amiot, M. Lewandowski, P. Leite, M. Thomas, and A. Perwuelz, *J. Mater. Sci.*, **49**, 52 (2014).
24. F. Farukh, E. Demirci, B. Sabuncuoglu, M. Acar, B. Pourdeyhimi, and V.V. Silberschmidt, *Compos. B Eng.*, **68**, 327 (2015).
25. X. Hou, M. Acar, and V.V. Silberschmidt, *Comput. Mater. Sci.*, **50**, 1292 (2011).
26. E. Sozumert, F. Farukh, E. Demirci, M. Acar, B. Pourdeyhimi, and V.V. Silberschmidt, *J. Phys. Conf. Ser.*, **628**, 012093 (2015).
27. F. Farukh, E. Demirci, B. Sabuncuoğlu, M. Acar, B. Pourdeyhimi, and V.V. Silberschmidt, *Comput. Mater. Sci.*, **71**, 165 (2013).
28. F. Farukh, E. Demirci, M. Acar, B. Pourdeyhimi, and V.V. Silberschmidt, *J. Mater. Sci.*, **49**, 4081 (2014).
29. D.V. Wilbrink, L.A.A. Beex, and R.H.J. Peerlings, *Int. J. Solids Struct.*, **50**, 1354 (2013).
30. H.S. Kim, A. Deshpande, B. Pourdeyhimi, A.S. Abhiraman, and P. Desai, *Text. Res. J.*, **71**, 157 (2001).
31. R. Chhabra, Composite filter substrate comprising a mixture of fibers. Google Patents, 2016.
32. J.H. Lin, T.T. Li, C.H. Huang, J.J. Ou, and C.W. Lou, *Appl. Mech. Mater.*, **749**, 253 (2015).
33. H.-C. Lien and C.-H. Liu, *Text. Res. J.*, **76**, 547 (2006).
34. R. Rezakhaniha, A. Agianniotis, J.T.C. Schrauwen, A. Griffa, D. Sage, C.V.C. Bouten, F.N. van de Vosse, M. Unser, and N. Stergiopulos, *Biomech. Model. Mechanobiol.*, **11**, 461 (2012).
35. H. Cox, *Br. J. Appl. Phys.*, **3**, 72 (1952).
36. E. Demirci, M. Acar, B. Pourdeyhimi, and V.V. Silberschmidt, *Comput. Mater. Sci.*, **52**, 157 (2012).
37. F. Farukh, E. Demirci, B. Sabuncuoglu, M. Acar, B. Pourdeyhimi, and V.V. Silberschmidt, *Int. J. Solids Struct.*, **51**, 1670 (2014).
38. R. Veerabadran, H.A. Davis, S.K. Batra, and A.C. Bullerwell, *Text. Res. J.*, **66**, 257 (1996).
39. R. Wijeratne, et al. *Text. Res. J.*, (2018). doi:10.1177/0040517517753640.